ADAPTIVE REGULARIZATION - A NEW METHOD FOR STABILIZATION OF SURFACE RECONSTRUCTION FROM IMAGES

Prof.Dr.-Ing. Bernhard P. Wrobel, Boris Kaiser, Julia Hausladen
Institute of Photogrammetry and Cartography
Technical University Darmstadt (Germany)
Washington 1992 - Comm. III

Abstract

Regularization of ill-posed image inversion problems using a stabilizing smoothing functional has one weak point: Breaklines (edges, creases, cusps, . . .) will not be properly reconstructed, if the parameters for smoothing are not chosen in an almost optimal way. Often curvature minimization is applied with global or local weighting. Global weighting tends to smoothen too much, whereas optimal local weighting is a crucial and time consuming operation. In this paper a smoothing functional is introduced using locally estimated curvatures and minimizing only their residuals together with a functional of image grey value residuals. The amount of object surface smoothing can be controlled by statistical tests. This procedure is called adaptive regularization. The impact of weights is of less importance than before. The basic equations are presented related to the object surface reconstruction approach called facets stereo vision (= FAST Vision). A series of experiments is presented at this congress in another paper from KAISER et al. 1992.

Key Words: DTM, Image Matching, Orthophoto, Rectification, 3-D

1. Introduction: Ill-Posed Problems and Regularization

Surface reconstruction as a problem of inverse optics belongs to the class of problems, which are ill-posed in the sense of Hadamard (TIKHONOV et al., 1977), i.e. at least one of the following conditions is not met by these problems:

existence of a solution, (1)
uniqueness of the solution (2)
stability: the solution depends continuously on the initial data. (3)

Problems not satisfying condition (1) may be called over-constrained, which is rarely the case in inverse optics. Problems, which do not fulfill one of the other two conditions (or both) can be regarded as under-constrained (BOULT, 1987). Meeting condition (3) does not ensure the robustness against noise in practice. Not meeting (3) means, that small changes in the initial data cause large ones in the results.

In order to provide numerical stability, the problem does not only have to be well-posed, but also be well-conditioned (POGGIO et al., 1985). Additional assumptions can turn ill-posed problems into well-posed ones. The use of supplementary information of a qualitative nature (e.g. smoothness of the solution) yields the regularization method (TIKHONOV et al., 1977). Taken more generally, the term regularization refers to any procedure turning ill-posed problems into well-posed ones. In computational optics ill-posedness is closely related to the occurrence of noise. Surface reconstruction requires regularization even in the absence of noise in order to bridge areas, in which the gradients of grey value signal are too low.

In order to restrict the space of solutions of a problem $Az = b$, a stabilizing functional $\|Bz\|$ is introduced:

find z, minimizing $\|Az - b\|^2 + \lambda \cdot \|Bz\|^2$, (4)

with λ, the regularization parameter. λ controls the compromise between regularization and data consistency. The qualitative assumption, expressed in the choice of a specific functional $\|Bz\|$, has to show physical plausibility. It is a very common approach to assume the reconstructed surface to be smooth. An oftenly used functional expressing this assumption is the quadratic variation (GRIMSON, 1981; TERZOPOULOS, 1988)

$$\|Bz\|^2 = \int\int (z_{xx}^2 + 2z_{xy}^2 + z_{yy}^2)\, dx\, dy. \qquad (5)$$

The surface reconstruction approach FAST Vision, used here, deals with discrete surface heights Z_{rs} as parameters in an XY-coordinate system. Thus, the stabilizing functional (5) has to be approximated by second differences, related to a set of facets (or grid) of the surface (figure 1.1):

$$\|Bz\|^2_{discr.} = \sum_r \sum_s \left(D^2_{xx}(Z_{rs}) + 2 \cdot D^2_{xy}(Z_{rs}) + D^2_{yy}(Z_{rs}) \right)$$

$$\text{with} \quad D_{xx}(Z_{rs}) = \frac{Z_{r+1,s} - 2Z_{rs} + Z_{r-1,s}}{h^2},$$

$$D_{xy}(Z_{rs}) = \frac{Z_{rs} - Z_{r+1,s} - Z_{r,s+1} + Z_{r+1,s+1}}{h^2} \qquad (6)$$

$$D_{yy}(Z_{rs}) = \frac{Z_{r,s+1} - 2Z_{rs} + Z_{r,s-1}}{h^2},$$

$$h = X_{rs} - X_{r-1,s} = Y_{rs} - Y_{r,s-1}$$

For some of the Z_{rs} (those situated in corners and edges) it is impossible to form all of the above mentioned equations, because some of the adjacent grid points are outside the window to be reconstructed. Such equations are simply omitted.

In the past, also functions of higher order differences of Z_{rs} have been proposed for stabilization. Twomey (see HUANG, 1975, pp. 187) found, that any constraint, which is quadratic in Z_{rs}, may be used to produce a solution resembling (4) with (6). This finding has been fairly well confirmed by RAUHALA et al., 1989, when computing a Digital Terrain Model (= DTM) from scattered Z-data and comparing 15 different constraining functions. So, one has to use one type of constraining function, but in general it is not decisive, which one.

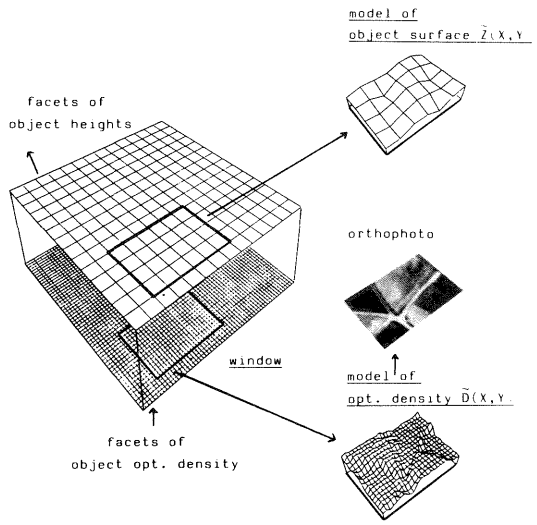

Fig. 1.1: FAST Vision: Simultaneous reconstruction of object surface $\tilde{Z}(X,Y)$ and optical object density $\tilde{D}(X,Y)$ or object grey value function $\tilde{G}(X,Y)$ resp.

However, the presence of breaklines in the surface or of other non-smooth surface elements and their reconstruction is the weak point for the application of such a functional. Applying the functional (6) with a large weight λ, can lead to errors, if the terrain to be reconstructed really is "rough". Surface edges may degenerate to arcs.

Since breaklines of topography or edges of workpieces play a fundamental role for morphologically correct reconstruction or for object recognition and for other postprocessing tools of object surface data, it has to be an ultimate goal to preserve these object characteristics as well as possible. Therefore, the following rule has to be pursued: As much regularization as necessary - as little regularization as possible. This rule emphazises the priority of data consistency in (4), and consequently, the necessity for optimal or near optimal local weights λ_{rs}, instead of one global parameter λ. In this context, there are many proposals (see HUANG, 1975, pp. 184, WEIDNER, 1991).

Now, the new regularization principle, given here, also relies on a curvature functional, but with a substantial difference to all approaches discussed so far: We do not regard the expectation of surface curvature to be zero. In our opinion, this assumption is true very rarely, both globally and locally. Therefore, the approximation to reality only by proper weighting is very crucial. In contrast to these approaches, we are introducing estimates of local surface curvature c with non-zero expectation. We are minimizing only their residuals together with the error functional of the image grey values, i.e.:

$$\text{find } z, \quad \text{minimizing } \|Az-b\|^2 + \lambda \|(Bz-c)\|^2 \qquad (7)$$

Here, the adaption to locally quickly changing surface curvatures will be obtained primarily by the estimated curvature values c themselves, as will be shown later. λ, now, is of minor importance.

The remainder of this paper is organized as follows: In section 2 a brief presentation of surface reconstruction by facets stereo vision (= FAST Vision) is given. Section 3 reports on numerical results of FAST Vision, stabilized only by proper choice of facets or by standard curvature minimization. The theory of the new method will be derived in section 4, and in section 5 numerical examples in comparison with the former methods will be demonstrated. Finally, section 6 contains some remarks on open questions.

2. Object Surface Reconstruction by Facets Stereo Vision (FAST Vision): The Basic Equations

Facets Stereo Vision is a method developed by Wrobel (WROBEL, 1987, 1991), which fulfills the task of simultaneous reconstruction of object surface Z(X,Y) and object grey value function G(X,Y). The relationship of a point on a surface and its images in the pictures P',P''... can be described with regard to radiometric and geometric characteristics. If the sensor, with which the picture was taken, is a metric camera, the geometric relation between the object coordinates X,Y,Z and the image coordinates x',y' in P' is given by the well-known perspective equations:

$$x' = x'_O - \frac{r_{11}\cdot(X-X_O)+r_{21}\cdot(Y-Y_O)+r_{31}(Z-Z_O)}{r_{13}\cdot(X-X_O)+r_{23}\cdot(Y-Y_O)+r_{33}(Z-Z_O)} \cdot c_K \qquad (8)$$

$$y' = y'_O - \frac{r_{12}\cdot(X-X_O)+r_{22}\cdot(Y-Y_O)+r_{32}(Z-Z_O)}{r_{13}\cdot(X-X_O)+r_{23}\cdot(Y-Y_O)+r_{33}(Z-Z_O)} \cdot c_K \qquad (9)$$

x'_O, y'_O and c_K are the interior orientation parameters, X_O, Y_O, Z_O and r_{ij} are the exterior orientation parameters. In this paper all these are assumed to be known.

The radiometric relation between an object grey value G(X,Y) and image grey values is modelled by linear transfer functions T', T'', . . ., which are invertable:

$$G(X,Y) = T'(G'(x',y')) = T''(G''(x'',y'')) = \ldots \qquad (10)$$

with G', G'' the grey values of pictures P', P'', ...

Of course, sensors with a different geometry can be chosen instead of (8), (9) and the transfer function does not have to be linear. Now, an image ray defined by the pixel coordinates x',y' and the perspective center X_O, Y_O, Z_O of image P' may intersect with an approximation of the surface at X^O, Y^O, Z^O. Then the expansion of G(X,Y) into a Taylor series leads to:

$$G(X^O+dX,Y^O+dY) = G(X^O,Y^O) + dG(X^O,Y^O) + \\ + \frac{\partial G(X^O,Y^O)}{\partial X} \cdot dX + \frac{\partial G(X^O,Y^O)}{\partial Y} \cdot dY \qquad (11)$$

Together with (10) this leads to:

$$G'(x',y') = T'^{-1}\left(G(X^O,Y^O) + dG(X^O,Y^O) + \right. \\ \left. + \frac{\partial G(X^O,Y^O)}{\partial X} \cdot dX + \frac{\partial G(X^O,Y^O)}{\partial Y} \cdot dY\right) \qquad (12)$$

The following equations, expressing the dependence of changes dZ in the Z-coordinates on changes dX, dY in X- and Y-coordinates, are known from analytical photogrammetry:

$$dX = \frac{\partial X}{\partial Z} \cdot dZ = \frac{X^O-X_O}{Z^O-Z_O} \cdot dZ = X'_Z \cdot dZ \qquad (13)$$

$$dY = \frac{\partial Y}{\partial Z} \cdot dZ = \frac{Y^O-Y_O}{Z^O-Z_O} \cdot dZ = Y'_Z \cdot dZ\,. \qquad (14)$$

Substituting (13) and (14) in (12) leads to:

$$G'(x',y') = T'^{-1}\left(G(X^O,Y^O) + dG(X^O,Y^O) + \right. \\ \left. + \frac{\partial G(X^O,Y^O)}{\partial X} \cdot X'_Z \cdot dZ + \frac{\partial G(X^O,Y^O)}{\partial Y} \cdot Y'_Z \cdot dZ\right) \qquad (15)$$

Now, the functions describing object surface and object grey values are introduced (see fig. 1.1). Up to now bilinear functions are used for each facet: for a surface or Z-facet and for a grey value or G-facet. The complete representation of object surface and the complete object grey value function by piecewise polynomial functions, depending on the unknown grid values Z_{rs} and G_{kl} can be written as:

$$G(X,Y) \approx \tilde{G}(X,Y) = \sum_k \sum_l \alpha_{kl}(X,Y) \cdot G_{kl} \qquad (16)$$

$$Z(X,Y) \approx \tilde{Z}(X,Y) = \sum_r \sum_s a_{rs}(X,Y) \cdot Z_{rs} \qquad (17)$$

with known functions $\alpha_{kl}(X,Y)$ and $a_{rs}(X,Y)$. Splitting of (16) into approximate values of the object grey values $\tilde{G}(X^O,Y^O)$ and their changes $d\tilde{G}(X^O,Y^O)$ leads to:

$$\tilde{G}(X^O,Y^O) = \sum_k \sum_l \alpha_{kl}(X^O,Y^O) \cdot G^O_{kl} \qquad (18)$$

$$d\tilde{G}(X^O,Y^O) = \sum_k \sum_l \alpha_{kl}(X^O,Y^O) \cdot dG_{kl}$$

Splitting of $\tilde{Z}(X,Y)$ can be done in an analogous way:

$$\tilde{Z}(X^O,Y^O) = \sum_r \sum_s a_{rs}(X^O,Y^O) \cdot Z^O_{rs}$$

$$d\tilde{Z}(X^O,Y^O) = \sum_r \sum_s a_{rs}(X^O,Y^O) \cdot dZ_{rs}$$

In equation (15) the partial derivatives of the grey value function are computed from (18):

$$\frac{\partial \tilde{G}(X^O,Y^O)}{\partial X} = \sum_k \sum_l \frac{\partial \tilde{G}(X^O,Y^O)}{\partial \alpha_{kl}(X^O,Y^O)} \cdot \frac{\partial \alpha_{kl}(X^O,Y^O)}{\partial X} \qquad (19)$$

$$\frac{\partial \tilde{G}(X^O,Y^O)}{\partial Y} = \sum_k \sum_l \frac{\partial \tilde{G}(X^O,Y^O)}{\partial \alpha_{kl}(X^O,Y^O)} \cdot \frac{\partial \alpha_{kl}(X^O,Y^O)}{\partial Y} \qquad (20)$$

From the above given relationships the fundamental differential equation of digital photogrammetry is obtained:

$$G'(x',y') = \\ T'^{-1}\left(\sum_k \sum_l \alpha_{kl}(X^O,Y^O) \cdot G^O_{kl} + \sum_k \sum_l \alpha_{kl}(X^O,Y^O) \cdot dG_{kl} + \right. \\ + \sum_k \sum_l \frac{\partial \tilde{G}(X^O,Y^O)}{\partial \alpha_{kl}(X^O,Y^O)} \cdot \left(\frac{\partial \alpha_{kl}(X^O,Y^O)}{\partial X} \cdot X'_z + \frac{\partial \alpha_{kl}(X^O,Y^O)}{\partial Y} \cdot Y'_z \right) \cdot \\ \left. \cdot \sum_r^m \sum_s^n a_{rs}(X^O,Y^O) \cdot dZ_{rs} \right) \qquad (21)$$

In order to reconstruct an object with the derived method at least a second picture is needed. The values associated with picture P' in (21) have to be replaced with those associated with the pictures P'',P''' etc. The evaluation of (21) for all pixels from all pictures leads to the following linear Gauß-Markov model:

$$E(l) = \underset{(n_o,n_n)}{A_l} \cdot x \qquad (22)$$

n_o is the number of observation equations of type (21) and $n_u \leq n_o$ is the number of unknowns: dG_{kl}, dZ_{rs} and the parameters of T', T'' etc. l is the vector of differences between the measured grey values G' and those grey values, which result from the approximate grey values of the object model:

$$G'(x',y') - T'^{-1}\left(\sum_k \sum_l \alpha_{kl}(X^O,Y^O) \cdot G^O_{kl} \right) \qquad (23)$$

This overdetermined problem can be solved by a least squares approach, which minimizes $v_l^T P_l v_l$ and which leads to the following system of normal equations:

$$A_l^T P_l A_l x = A_l^T P_l l. \qquad (24)$$

P_l is the weight matrix associated with the observed image grey values.
As can be realized from equation (21), FAST Vision is a non-linear problem and the solution of (24) may be computed by Newton-Gauß iteration. For latest details concerning FAST Vision see (WEISENSEE, 1991).

From now on, but only in this paper, not in practice, we suppose, that the parameters of the transfer functions T', T''... are already given. Then, the matrix A_l consists of two submatrices: the coefficient matrix A_Z for the unknowns x_Z of the object surface and the coefficient matrix A_G for the grey value unknowns x_G:

$$A_l = (A_G \; A_Z).$$

As the elements of A_Z depend on the partial derivatives of the grey values, see (12) and (21), linear dependences of some columns of this submatrix can occur, if the measured grey values are constant in larger regions of the pictures, or if they increase or decrease linearly in X-Y-space. This will cause the product

$$A_1^T P_1 A_1 = \begin{pmatrix} A_G^T P_1^T A_G & A_G^T P_1 A_Z \\ A_Z^T P_1 A_G & A_Z^T P_1 A_Z \end{pmatrix}$$

to become a singular or at least an ill- conditioned matrix. In that case the image inversion problem cannot be solved by the equations (21) alone, unless additional observation equations are added in a well-defined procedure of regularization.

3. Regularization of FAST Vision by Choice of Appropriate Facets and by Curvature Minimization

Sufficient regularization may already be obtained by choice of the appropriate size of facets. Indeed, for the representation of the object grey value function $\tilde{G}(X,Y)$ in relationship (21) a constant ratio of 2x2 pixels per G-facet has been found to be a reasonable compromise between resolution and accuracy. This ratio can be used everywhere. It is independent of the image signals, as long as pixel size itself is in correct relation to image signal. In contrast to this Z-facets should have a variable size in principle, in one window already, because the Z-parameters in (21) depend exclusively on the grey value gradient, which is a space function of X, Y. The realization of that optimal idea seems to be too complicated. We decided for a constant size of Z-facets in combination with stabilizing constraints with local weights. This approach has many advantages as will come out in this paper.

In this section the limitation of two simple stabilizing methods will be demonstrated: stabilization only by constant, rather large Z-facets and by curvature minimization with global weights.

The numerical experiments in this section are performed with two stereo image pairs, generated of the same object. It can be described as a gable roof: two planes with an inclination of 20° meet at a ridge. There is a shady plane containing the grey values from 0 to 127, and a plane exposed to the light containing grey values from 128 to 255. The simulated photographs of the object were taken with a standard deviation of 4 grey values (white noise), pixel size is 20 µm × 20 µm. This is the first image pair used in the first experiment. The following photogrammetric parameters are the same for both image pairs: image scale 1:12000, base-to-height ratio 1:1.6, for comparison with standard accuracy of today's photogrammetry: 0.1 °/oo D = 0.18 m, with D = distance object-image.

The second image pair has been generated with a slightly different texture (see fig. 3.1): In the centre of the object, there is a 5×5 Z-facets region containing the grey value constant 127.

The parameters chosen for the FAST Vision process are:

size of Z-facets 2m x 2m
G-facets per Z-facet 4 x 4
pixel per G-facet 2.083 x 2.083 .

The 12×12 Z-facets, which were selected for surface reconstruction, are located on both sides of the ridge (c. fig. 3.1), and the ridge coincides with the boundary of Z-facets.

In all experiments, the iterations of FAST Vision are started from a horizontal surface plane through the roof.

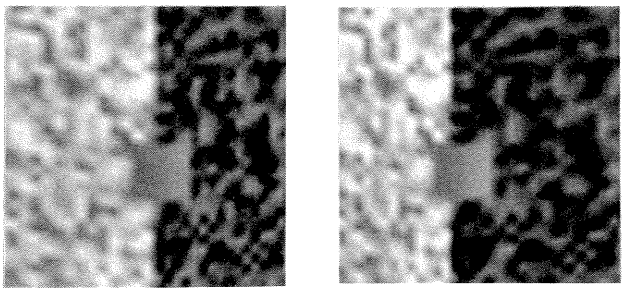

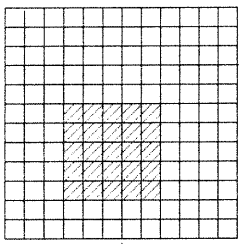

Fig. 3.1: Generated pictures and position of the ridge within the Z-facets. The hatched facets represent the region with constant grey values.

In the first experiment only the grey value equations (21) have been evaluated, thereby applying the following simple regularization procedure: increase the size of Z-facets till sufficient stability has been obtained. All the other parameters of FAST Vision have been kept fixed.

Results:

We started with the above mentioned size of 2m x 2m, but convergence was obtained not before a Z-facet size of 5m x 5m. Here, stabilization has to be paid by poor resolution. However, the accuracy figures, computed from least squares, are very good: standard deviation s_0 of the observations G', G'': s_0 = 3.97 grey values (a priori s_0 = 4), mean $\bar{s}_Z$ of the standard deviations of all Z: $\bar{s}_Z$ = 0.042 m, which is in good agreement with the root mean square of true Z-errors: rms (dZ) = 0.068 m.

The second experiment shows the performance of regularization by curvature minimization. The second image pair (fig. 3.1) and all the other parameters, given above, have been introduced. For regularization only global weights λ have been used.

Results (see fig. 3.2 and 3.3):

The Z-resolution has been improved from 5m x 5m to 2m x 2m, but at the expense of a rather high regularization parameter λ. No convergence is obtained with λ=2000. Fig. 3.3 shows, that the ridge (roofline) is flattened by a high regularization parameter λ. The region with constant grey values lowers the ridge at this point. Both effects can be seen clearly in the dZ-graph. In the region of constant grey values, there are no deterministic grey value gradients, only very small stochastic gradients, resulting from grey value noise. Nevertheless, it is possible to reconstruct the surface in that region, but only with high regularization parameter λ. High λ - on the other hand - has a rather far extending impact on the surroundings of each Z_{rs}, as can be seen from the distribution of positive and negative dZ-values, see fig. 3.3. Also, there is only a weak agreement of $\bar{s}_Z$ with rms (dZ). Regularization by curvature minimization with global weights is not satisfying.

λ	s_o	rms(dZ)	$\bar{s}_z$	n_i
6000	4.260	0.245	0.0304	13
2000	no convergence			

λ	global regularization parameter
s_o	standard deviation of unit weight (in grey values)
rms(dZ)	root mean square of true Z-errors [metres]
$\bar{s}_z$	mean of standard deviations of Z-unknowns [metres]
n_i	number of iterations on zero level of image pyramid

Fig. 3.2: Experimental results for regularization with curvature minimization

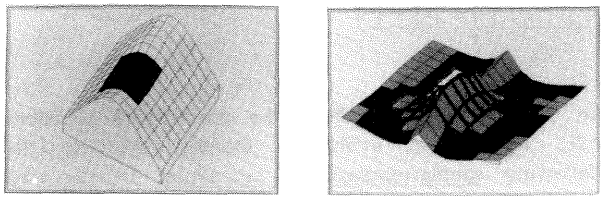

Fig. 3.3: Regularization with curvature minimization: Reconstructed roofline with $\lambda = 6000$ (left) and dZ-graph (right).
dZmax = +1.118 m and dZmin = - 0.335 m; the dark facets represent the region with constant grey values (left) and facets with dominant negative differences (right)

4. Adaptive Regularization of FAST Vision

This new method refers to relationship (7). Actually, it is based on a proposal given earlier by Wrobel (WROBEL, 1973, 1974) for stabilization of ill-conditioned linear systems. Here, use is made of the curvature constraints (6) for every Z-facet as in section 3, however, with curvature values c, that are estimated from grey value observables during the reconstruction process.

4.1 Derivation of an Iterative Method for Regularization with Constraints

There are several computational procedures (WROBEL, 1974) to solve the basic approach. Here, we present a very simple one.
To fulfill functional (7), a system of two groups of observation equations is set up:

$$v = \begin{pmatrix} v_1 \\ v_2 \end{pmatrix} = \begin{pmatrix} A_1 & 0 \\ A_2 & I \end{pmatrix} \cdot \begin{pmatrix} x \\ c \end{pmatrix} - \begin{pmatrix} l_1 \\ 0 \end{pmatrix}; \quad P = \begin{pmatrix} P_1 & 0 \\ 0 & P_2 \end{pmatrix} \qquad (25)$$

For later use we set $A = \begin{pmatrix} A_1 & 0 \\ A_2 & I \end{pmatrix}$, with I = unit matrix.

The first group originates from the n_o observation equations of the FAST Vision method, derived from the image grey values, see (21). The second group comprises the n_a additional from discrete curvature equations at the facets, with c the unknown vector of curvatures. A_2 is formed by D_{xx}, D_{xy} and D_{yy}, obtained with (6) from the Z-facets at the start of each FAST Vision iteration step, P_2 is a diagonal matrix, representing local regularization parameters λ.
The minimization of v^TPv leads to:

$$\begin{pmatrix} A_1^TP_1A_1+A_2^TP_2A_2 & A_2^TP_2 \\ P_2A_2 & P_2 \end{pmatrix} \cdot \begin{pmatrix} x \\ c \end{pmatrix} - \begin{pmatrix} A_1^TP_1l_1 \\ 0 \end{pmatrix} = 0 \qquad (26)$$

From the second line of (25) and of (26) follows:

$$v_2 = 0$$

This leads to:

$$v^TPv = v_1^TP_1v_1 , \qquad (27)$$

i.e. the residuals of the original observation equations $v_1 = A_1x - l_1$ are also the residuals of the extended system (25). Similarly, it can be shown that

- x from system (26) is equal to $x_1 = (A_1^TP_1A_1)^{-1}A_1^TP_1l_1$,
- Q_{xx}, the cofactor matrix of x from the inversion of (26) is equal to $(A_1^TP_1A_1)^{-1}$,
- and, finally, the redundancy of system 1 is the same as that of the enlarged system (26).

Now, the numerical solution of system (26) can be performed to advantage by the block Gauß-Seidel iterative method (WROBEL, 1974). The first iteration step (o) is started with an arbitrary vector $x^{(o)}$. The second line of (26) is solved for $c^{(o)}$, while $x^{(o)}$ is kept constant: $c^{(o)} = -A_2x^{(o)}$. Then the first line of (26) with $c^{(o)}$ as a constant, is solved for $x^{(1)}$:

$$x^{(1)} = (A_1^TP_1A_1+A_2^TP_2A_2)^{-1} \cdot (+A_1^TP_1l_1 - A_2^TP_2c^{(o)}).$$

The full rank of $A_1^TP_1A_1$ cannot be guaranteed, but the sum $(A_1^TP_1A_1+A_2^TP_2A_2)^{-1}$ has been made invertable through regularization.

On the i-th iteration step, with $B = A_1^TP_1A_1+A_2^TP_2A_2$, the solution for the unknowns $x^{(i+1)}$, $c^{(i)}$ reads:

$$c^{(i)} = -A_2x^{(i)} \qquad (28)$$
$$x^{(i+1)} = B^{-1} \cdot (A_1^TP_1l_1 - A_2^TP_2c^{(i)}). \qquad (29)$$

Substituting $c^{(i)}$ according to (28) in (29), results in a blockwise Gauß-Seidel iteration method for computing x:

$$x^{(i+1)} = B^{-1} \cdot A_2^TP_2A_2x^{(i)} + B^{-1}A_1^TP_1l_1 = Gx^{(i)} + B^{-1}A_1^TP_1l_1. \qquad (30)$$

G is called the iteration matrix of the method and the method itself is called adaptive regularization. In every iteration step (i), we also may compute the residual vectors $v_1^{(i)}$ and $v_2^{(i)}$, by inserting $x^{(i)}$ and $c^{(i)}$ in (25). From these vectors the following statistical functions are derived:

$$\frac{(v_1^TP_1v_1)^{(i)}}{n_o - n_u} = (s_1^{(i)})^2 \qquad (31)$$

$$\frac{(v_2^TP_2v_2)^{(i)}}{n_a} = (s_2^{(i)})^2 . \qquad (32)$$

$s_1^{(i)}$ is the standard error of unit weight of an observation

in group 1 and $s_2^{(i)}$ in analogy for group 2. For FAST Vision $s_1^{(i)}$ characterizes the goodness of fit for the grey values and $s_2^{(i)}$ the still inherent amount of smoothing of the surface. These quantaties may be used for quality control of the reconstruction results during iteration.
If convergence exists, then in the limit, for $i \rightarrow \infty$, we obtain (irrespective of P_2!):

$$\begin{aligned} x^{(i)} &\rightarrow x_1 \\ c^{(i)} &\rightarrow c \\ v_1^{(i)} &\rightarrow v_1 \\ v_2^{(i)} &\rightarrow 0 \end{aligned} \qquad (33)$$

The results (33) are not influenced by P_2, the weights of curvature equations, but speed of convergence and the condition number of the main matrix in (26) are depending on P_2 (WROBEL, 1974).
For quality control, the standard errors of $x^{(i)}$, derived from the inverse of $(A_1^T P_1 A_1)$, may be determined according the same iteration scheme (WROBEL, 1974).

However, the success and complete characteristics of the iteration process, described so far, will depend upon the iteration matrix G and the matrices behind it: $G = (A_1^T P_1 A_1 + A_2^T P_2 A_2)^{-1} A_2^T P_2 A_2$. As has been shown in detail in WROBEL et al. 1991 their properties are formed in essence by the rank and condition number of matrix $A_1^T P_1 A_1$, originating from the grey value equations. There are two cases, and they give rise to two variants, of which adaptive regularization is composed of: self adaptive regularization and pyramid assisted regularization.

4.2 Adaptive Regularization

FAST Vision is started with self adaptive regularization, applying a global weight matrix $P_2 = \lambda I$ for the constraints. λ should be chosen as low as possible. This, already, can produce the final result, if matrix $(A_1^T P_1 A_1)$ has full rank and an acceptable stability. The solution vector $x^{(i)}$ converges to the correct solution, irrespective of P_2. If the iteration tends to $i \rightarrow \infty$, there is no smoothing, as can be seen from relationships (33). As long as $i < \infty$, the qualitiy of surface reconstruction can be controlled by statistical tests:

- The standard error of unit weight, $s_1^{(i)}$, see (31), may be compared with s_1 a priori, in order to check the goodness of fit of the reconstructed grey value function $\tilde{G}(X,Y)$, see (16), to the given image grey values G', G''...
- Additionally, the amount of smoothing, which is inherent in the surface at iteration step (i), may be checked by comparison of the mean curvature residuals $s_2^{(i)}$, (32), with zero or with an alternative figure greater than zero. With respect to the statistical errors of the reconstructed surface smoothing can be tolerated to some extent.

However, the conditions of self adaptive regularization will hardly exist in an entire object window. As discussed earlier, weak or zero grey value gradients give rise to the situation, that some of the parameters Z_{rs}, somewhere in the window, are very badly or even not at all determinable. Then, matrix $(A_1^T P_1 A_1)$ is ill-conditioned or even not of full rank. The solution vector $x^{(i)}$ still converges, irrespective of P_2, but it will depend upon the start vectors $x^{(0)}$ and $c^{(0)}$. This has been shown in WROBEL et al. 1991. Therefore, this solution cannot be accepted in general. So, all parameters Z_{rs} have to be examined, whether they can be accepted (= step 1) or whether they deserve more stabilization (= step 2). We sketch a procedure in short lines, with which the problem can be overcome.

Step 1: Localization of unstable Z_{rs}
Compute the standard errors of Z_{rs} from the stabilized equations (26), and compare them with corresponding standard errors from constraining equations alone. Z_{rs}, with statistically significant differences in those errors, are supposed to be stable. They will be accordingly processed in step 2. However, often the matrix of constraints $(A_2^T P_2 A_2)$ is not invertible. In that case a relative comparison of the standard errors, computed from the stabilized system is possible, in any way: All standard errors are compared with the smallest standard error $s(Z_{rs})_{min}$ or with another reasonable threshold from experience. Z_{rs}, with a standard error greater than the threshold by a constant of about 5, say, are regarded as unstable. The appropriate definition of suitable thresholds is already a matter of application. It will be discussed elsewhere.

Step 2: Pyramid assisted regularization of unstable Z_{rs}.
By that procedure, the curvature values c of unstable Z_{rs} will not any more be estimated in the least squares procedure as unknown parameters. By contrast, they are given 'reasonable' curvature values as 'observations', zero values, say, and are processed accordingly in FAST Vision. We prefer curvature values, derived from the surroundings of unstable Z_{rs} by interpolation. For FAST Vision, this simply means to use curvature values from the next higher level of surface pyramid. This variant of adaptive regularization, therefore, is called pyramid assisted regularization.
To be more precise, those 'reasonable observations' of curvature, of course, are arbitrary information and may produce not very reliable facets. In view of photogrammetric practice, these facets could be marked by the computer and be inspected by an operator.
To bring the overall procedure to an end, after step 2, the computations of FAST Vision are repeated with the now two classes of facets.
It may be argued, the final result will be influenced by the choice of $P_2 = \lambda I$ at the beginnning. This objection is not true for the solution vector, but the standard errors are perturbed by the constraints: they are always too low. The numerical example in fig. 3.2 has shown this already. However, if reliable quality assessment for each parameter Z_{rs} is a strict demand, the following step 3 may be performed.

Step 3: Refinement of standard errors of parameters Z_{rs}.
The amount of λ in $P_2 = \lambda I$ at the beginning has had to stabilize the weakest parameters Z_{rs}. After step 2, these are made very stable, so λ may be substantially lowered. Again, this may be pursued globally, but could be done also locally in relation to the individual standard errors of Z_{rs}, which have been computed already in step 2. So, finally, the above mentioned rule - regularization as little as possible - can be realized.

5. Numerical Experiments Of FAST Vision With Adaptive Regularization

In this paper only introducing experiments are presented. However, in another paper at this congress a series of different examples is given, see KAISER et al. 1992.
In order to compare the methods of regularization the experiment of chapter 3 is carried out again. The second pair of images (with a section of constant grey value) was used. The photogrammetric and FAST Vision parameters are the same as in chapter 3.. An image pyramid with two levels was applied. The results of the experiments in fig. 5.1 - 5.3 correspond to those in chapter 3, see fig. 3.2 for explanation.

λ	s_0	rms(dZ)	$\bar{s}_Z$	n_i
6000	3.914	0.152	0.0279	12
2000	3.910	0.154	0.0373	12
2000	3.901	0.200	0.0368	66
6000	3.917	0.158	0.0279	11
2000	3.911	0.152	0.0373	11
2000	3.906	0.182	0.0369	65

Fig. 5.1: Experimental results: exclusively self adaptive regularization (above), combined self adaptive and pyramid assisted regularization (below)

Results:

- The quality of reconstruction is definitely better than with curvature minimization, fig. 3.2, at the same number of iterations! The true errors dZ at the roofline have the same magnitude as everywhere, with the exemption of the region with constant grey values. This region is not correctly reconstructed (nothing else had to be expected because of lacking deterministic grey values). But in these experiments the differences between the true and the reconstructed object are smaller than with curvature minimization (v. fig. 5.2 and fig. 5.3). This indicates a better interpolation in that region, due to the use of approximated curvature values from surface pyramid, being closer to reality than in the case of regularization by curvature minimization. So, FAST Vision with adaptive regularization shows up remarkable edge preserving characteristics.
- As predicted by theory in section 4.1, see (33), the results of true errors dZ and standard error s_0 practically do not differ with different regularization weight $P_2 = \lambda I$, fig. 5.1.
- Also, the impact of different iteration numbers n_i is confirmed as predicted. The reconstructed surface becomes rougher with increasing n_i. The true errors dZ are distributed more stochastically - as they should do (cf. white image noise) - than with low iteration numbers n_i. This effect results from the smoothing influence of the additional observation equations (see chapter 4.1), which decreases with n_i.

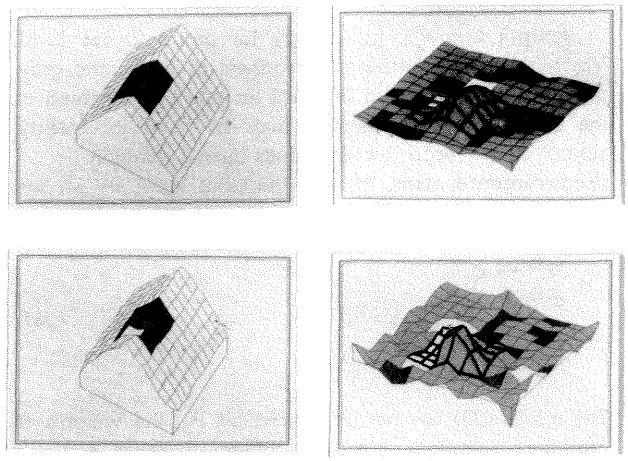

Fig. 5.2: Reconstructed roofline: self adaptive regularization (left) and dZ-graph (right)
$\lambda = 6000$, dZmax = +0.873m and dZmin = -0.195 m, 12 iterations (above)
$\lambda = 2000$, dZmax = +1.059m and dZmin = -0.647m, 66 iterations (below)

- However, the mean but not the maximum difference between true and reconstructed object gets larger with increasing number of iterations. This seems to be a paradoxical result, but it corresponds to the special shape of the object, which consists of two planes. Therefore, this result probably cannot be generalized to other surfaces.
- The results of self adaptive and of pyramid assisted regularization can be compared in region of constant grey values, v. fig. 5.2 and 5.3. They do not differ much in that experiment. The average standard error $\bar{s}_Z$ does not agree with the corresponding rms of true errors. This discrepancy could be removed, if the refinement procedure for standard errors, see section 4.2, step 3, is used subsequently.

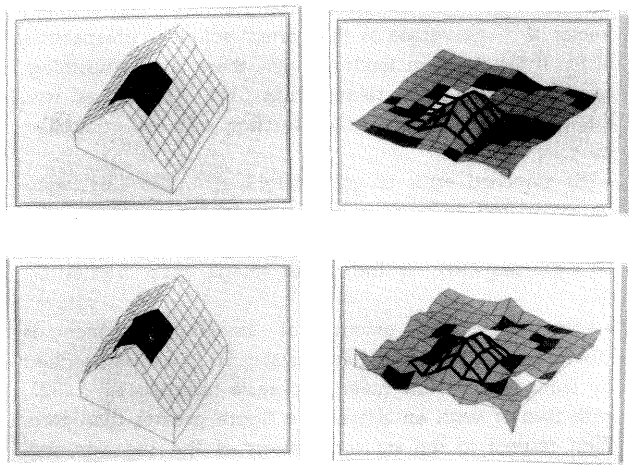

Fig. 5.3: Reconstructed roofline: combined self adaptive and pyramid assisted regularization (left) and dZ-graph (right):
$\lambda = 6000$, dZmax = +0.892 m and dZmin = -0.201 m, 11 iterations (above)
$\lambda = 2000$, dZmax = +0.819 m and dZmin = -0.639m, 65 iterations (below)

6. Conclusions

The theory of a stabilizing method for ill-posed problems has been given, applied for object surface reconstruction by FAST Vision and tested with some first experiments. In comparison to the often used procedure of curvature minimization, the following merits have evolved:

- Surface reconstruction is definitely better, especially the reconstruction of edges or breaklines.
- The results do not depend as much on the regularization parameters as they do with curvature minimization. So, the time consuming determination of local regularization parameters is not necessary.
- The standard errors of the results are still directly affected by the regularization parameter. But with additional computer work, refined and more reliable standard errors may be computed.
- In general, statistically well defined accuracy measures are at hand, since the approach is modeled as a Gauß-Markov estimation.

Finally, the theory of adaptive regularization, section 4.1, may be transfered to other problems with ill-posedness or ill-conditioning, e.g. least squares image matching or self-calibration of analytical photogrammetry.

7. References

Boult, T.E., What is Regular in Regularization. Proceedings of the 1st International Conference on Computer Vision, p.p. 457-462, London, 1987

Huang, T.S. (ed.), Image Enhancement and Restoration, Picture Processing and Digital Filtering. Springer Verlag, Berlin Heidelberg New York, 1975

Grimson, W.E.L., From images to Surfaces: A Computational Study of the Human Early Visual System. MIT Press, Cambridge, MA, 1981

Kaiser, B. / Wrobel, B. / Hausladen, J. / Tsay, J.-R., Application of FAST Vision for Digital Terrain Model Generation. Presented Paper, XVIIth Congress of ISPRS, Comm. III/2, Washington 1992

Poggio, T./Torre, V./Koch, C., Computational Vision and Regularization Theory. Nature Vol. 317, p.p. 139-155, 1985

Rauhala, U.A./ Davis, D./ Baker, K., Automated DTM Validation and Progressive Sampling Algorithm Of Finite Element Array Relaxation. Photogrammetric Engineering and Remote Sensing, Vol. 55, No. 4, pp. 449-465, 1989

Terzopoulos, D., The Computation of Visible Surface Representations. PAMI, Vol. PAMI-10, No. 4, p.p.417-438, July 1988

Tikhonov, A.N./Arsenin, V.Y., Solutions of Ill-Posed Problems. V.H. Winston & Sons, Washington D.C., 1977

Weidner, U., Informationserhaltende Filterung digitaler Bilder und ihre Bewertung. Mustererkennung 1991, Springer Verlag, Berlin, 1991

Weisensee, M., Modelle und Algorithmen für das Facetten-Stereosehen. Deutsche Geodätische Kommission, Reihe C, Nr. 374, München, 1991

Wrobel, B., On refinements of least squares solutions by improving the condition number using additive modifications. Intern. Symp. on Comp. Methods in Geodesy, Oxford, 1973

Wrobel, B., Zur Steigerung der Auflösungsgenauigkeit von Normalgleichungen durch Konditionsverbesserung mittels additiver Modifikation. Deutsche Geodätische Kommission, Reihe C, Nr 199, München, 1974

Wrobel, B., Digital Image Matching by Facets Using Object Space Models. 4th International Symposium on Optical and Optoelectr. Appl. Science and Engineering, March 30th-April 3rd 1987, The Hague, Netherlands, SPIE 804, p.p. 325-333

Wrobel, B., The Evolution Of Digital Photogrammetry From Analytical Photogrammetry. Photogrammetric Record, 13(77), p.p. 765-776, April 1991

Wrobel, B. / Kaiser, B. / Hausladen, J., Adaptive Regularization of Surface Reconstruction By Image Inversion. In: Förstner, W./ Ruwiedel, St. (eds) : Robust Computer Vision. Wichmann Verlag, Karlsruhe 1992

These investigations are supported by Deutsche Forschungsgemeinschaft.